tween peaks A and B in Fig. 2B is consistent with Alvin observations in December 1993 of waning hydrothermal activity along much of this ridge crest area (*31*).

REFERENCES AND NOTES

1. K. L. Von Damm, *Geophys. Monogr. Am. Geophys. Union* **91**, 222 (1995).
2. C. Lalou *et al.*, *J. Geophys. Res.* **98**, 9705 (1993).
3. D. Kadko, *Rev. Geophys.* **34**, 349 (1996).
4. H. Elderfield and A. Schultz, *Annu. Rev. Earth Planet. Sci.* **24**, 191 (1996).
5. T. M. Shank *et al.*, *Eos* **76**, F701 (1995).
6. D. Fornari, F. Voegeli, M. Olsson, *RIDGE Events* **7**, 13 (1996).
7. J. S. Killingley, W. H. Berger, K. C. MacDonald, W. A. Newman, *Nature* **287**, 218 (1980).
8. M. Roux, M. Rio, E. Fatton, *Bull. Biol. Soc. Wash.* **6**, 211 (1985).
9. G. Roesijadi and E. A. Crecelius, *Mar. Biol.* **83**, 155 (1984).
10. C. Chassard-Bouchaud, A. Fiala-Medioni, P. Galle, *C. R. Acad. Sci.* **302**, 117 (1986).
11. The Cameca 3f ion probe at Woods Hole Oceanographic Institution was used for all Sr/Ca analyses and follows the technique of (*36*). Spot size was 30 to 40 μm. Drift and intercalibration utilized a natural calcite standard mounted with each specimen. The accuracy of a single spot analysis is better then ±1.6% (2σ). The ion ratio conversion is Sr/Ca mole ratio = 0.00771 $^{88}Sr/^{42}Ca$ ion ratio.
12. S. R. Hart and J. Blusztajn, in *Seventh Annual V. M. Goldschmidt Conference, LPI Contribution No. 921* (Lunar and Planetary Institute, Houston, 1997), p. 89.
13. C. R. Fisher *et al.*, *Deep Sea Res.* **35**, 1811 (1988).
14. R. R. Hessler, W. M. Smithey, C. H. Keller, *Bull. Biol. Soc. Wash.* **6**, 411 (1985).
15. V. Tunnicliffe, *Oceanogr. Mar. Biol. Annu. Rev.* **29**, 319 (1991).
16. R. A. Lutz and M. J. Kennish, *Rev. Geophys.* **31**, 211 (1993).
17. M. Rio and M. Roux, *C. R. Acad. Sci.* **299**, 167 (1984).
18. R. A. Lutz, L.W. Fritz, D. C. Rhoads, *Biol. Soc. Wash. Bull.* **6**, 199 (1985).
19. R. A. Lutz, L. W. Fritz, R. M. Cerrato, *Deep Sea Res.* **35**, 1793 (1988).
20. K. K. Turekian and J. K. Cochran, *Science* **214**, 909 (1981).
21. ——, J. T. Bennett, *Nature* **303**, 55 (1983).
22. M. J. Kennish, R. A. Lutz, A. S. Pooley, *RIDGE Events* **8**, 6 (1997).
23. A Sr/Ca record for 1956 to 1963 was determined for a 38-year-old *Arctica islandica* collected in 1991 at 60-m depth near the Nantucket Shoals Lightship. See (*37*) for a $\delta^{18}O$ time series. Weekly bottom water temperature records for this site were matched with Sr/Ca amplitudes to give a temperature calibration of T°C = 20,752 [Sr/Ca (mol/mol)] − 16.0. Slope and intercept errors of the regression line are ±9.6% and ±3.0°C (1σ).
24. J.-J. Oberling and K. J. Boss, *Rev. Suisse Zool.* **77**, 81 (1979).
25. K. J. Boss and R. D. Turner, *Malacologia* **20**, 161, (1980)
26. B, F, Mg, Sr, and Ba contents in a 2-year interval in the *Arctica* specimen were similar (5 to 30%) to the 1975 to 1979 segment of *Calyptogena* 2498.
27. R. M. Haymon *et al.*, *Earth Planet. Sci. Lett.* **119**, 85 (1993).
28. K. H. Rubin, J. D. Macdougall, M. R. Perfit, *Nature* **368**, 841 (1994).
29. The 21°N EPR age model (*19*) is as follows: age = −20.921 ln[1.0222 − 0.00946 × height (mm)].
30. The fluid Sr/Ca ratio is not independent of temperature because the Sr/Ca of the diffuse fluid end member is ~34% that of ambient seawater (*38*). At 20°C, this effect is −0.38% per °C; the temperature dependence is +2.3% per °C. Our temperatures may be underestimated by up to 10°C at 50°C.
31. T. M. Shank *et al.*, *Deep Sea Res.*, in press.
32. J. J. Childress, C. R. Fisher, J. A. Favuzzi, N. K. Sanders, *Physiol. Zool.* **64**, 1444 (1991).
33. M. J. Kennish and R. A. Lutz, *Rev. Aquat. Sci.* **6**, 29 (1992).
34. Z. Liu and W. Dreybrodt, *Geochim. Cosmochim. Acta* **61**, 2879 (1997).
35. The 1991 to 1992 growth rate occurs at the same age as the observed 1991.5 height when height = 107 − 104.65 exp(− 0.0363t).
36. S. R. Hart and A. L. Cohen, *Geochim. Cosmochim. Acta* **60**, 3075 (1996).
37. C. R. Weidman, G. A. Jones, K. C. Lohmann, *J. Geophys. Res.* **99**, 18305 (1994).
38. R. H. James and H. Elderfield, *Geology* **24**, 1147 (1996).
39. D. J. Fornari, R. M. Haymon, M. R. Perfit, T. K. Gregg, M. H. Edwards, *J. Geophys. Res.*, in press.
40. D. Fornari, T. Shank, R. Lutz, unpublished data.
41. We are indebted to D. Fornari for his many unselfish contributions to this project. The in situ temperature data were generously provided by D. Fornari, R. Lutz, and T. Shank. Discussions, comments, and reviews by D. Fornari, G. Ravizza, L. Mullineaux, and K. Turekian were most helpful. This work was carried out with the support of the C. O. Iselin Chair.

20 October 1997; accepted 13 March 1998

Pressure-Induced Amorphization and Negative Thermal Expansion in ZrW_2O_8

C. A. Perottoni and J. A. H. da Jornada*

It has recently been shown that zirconium tungstate (ZrW_2O_8) exhibits isotropic negative thermal expansion over its entire temperature range of stability. This rather unusual behavior makes this compound particularly suitable for testing model predictions of a connection between negative thermal expansion and pressure-induced amorphization. High-pressure x-ray diffraction and Raman scattering experiments showed that ZrW_2O_8 becomes progressively amorphous from 1.5 to 3.5 gigapascals. The amorphous phase was retained after pressure release, but the original crystalline phase returned after annealing at 923 kelvin. The results indicate a general trend between negative thermal expansion and pressure-induced amorphization in highly flexible framework structures.

Pressure-induced amorphization is a phenomenon of widespread occurrence among framework structures, and many recent theoretical and experimental investigations have been devoted to extending our understanding of the underlying mechanisms (*1*, *2*). Disordered phases can be generated upon compression and decompression and even during indentation hardness tests (*2*, *3*). Several mechanisms have been proposed to explain the process of pressure-induced amorphization in solids, including melting effects and kinetically frustrated phase transitions to another crystalline state, as well as the failure of some criterion of lattice stability (*1*, *2*). Some compounds, including ice and silicon, that under special conditions transform to an amorphous phase under pressure also exhibit negative thermal expansion, at least within a limited range of temperature. Recent computer simulations pointed out the possibility of a common origin between pressure-induced amorphization and negative thermal expansion in tetrahedrally bonded networks (*4*).

The remarkable behavior of ZrW_2O_8, a cubic compound that contracts on heating, has been known for the past 30 years (*5*). Recent measurements have shown that ZrW_2O_8 exhibits isotropic negative thermal expansion over its entire range of stability, from 0.3 to 1050 K (*6*, *7*). This property makes zirconium tungstate an ideal candidate for investigating the relation between contraction on heating and pressure-induced amorphization in framework structures.

The crystal structure of ZrW_2O_8 at ambient conditions can be described as a framework of corner-sharing ZrO_6 octahedra and WO_4 tetrahedra. In each WO_4 tetrahedron, one of the oxygen atoms is bonded to only one tungsten atom, resulting in a structure with great flexibility. This compound undergoes a structural phase transition at about 430 K, from space group $P2_13$ to $Pa\bar{3}$, which hardly affects the negative thermal expansion coefficient (*6*, *7*). Recently, Evans and co-workers showed that upon compression above 0.2 GPa, cubic ZrW_2O_8 transforms to a quenchable orthorhombic phase (space group $P2_12_12_1$), which also exhibits negative thermal expansion, although reduced by one order of magnitude (*8*).

The great flexibility of the ZrW_2O_8 framework seems to be the key to its unusual properties (*9*). Because of this high flexibility, some low-energy vibrational modes can propagate through the structure without distortion of the ZrO_6 and WO_4 building blocks. These vibrational modes, called rigid unit modes (RUMs), have been successfully applied to the study of properties

---

Universidade Federal do Rio Grande do Sul, Instituto de Física, 91501-970 Porto Alegre-RS, Brazil.

*To whom correspondence should be addressed. E-mail: jornada@if.ufrgs.br

and phase transitions of several framework structures (*10*). In the case of ZrW_2O_8, the mechanism proposed to explain the negative thermal expansion involves low-frequency RUMs and QRUMs (quasi-RUMs or modes that propagate with slight deformation of the polyhedral units) with wave vectors distributed over a complicated three-dimensional surface in reciprocal space (*9*).

The powder sample of ZrW_2O_8 used in this work was prepared according to the procedure described in the literature (*11*). The pressure behavior of ZrW_2O_8 was investigated at ambient temperature (about 300 K) by in situ energy-dispersive x-ray diffraction (EDXRD) and Raman spectroscopy (*12*, *13*). Pressure was generated in a diamond anvil cell (DAC) and measured with the ruby fluorescence technique (*14*, *15*). Large samples were processed with a toroidal chamber (*16*, *17*).

EDXRD patterns of ZrW_2O_8 were acquired for pressures up to 8 GPa (Fig. 1). Except for a shift in peak positions, the transition from cubic to orthorhombic phase above 0.2 GPa did not alter the general appearance of the x-ray diffraction pattern substantially, at least within the experimental limitations imposed by the resolution of the energy-dispersive technique. The diffraction peaks became progressively broadened above 1.8 GPa, and at 3.5 GPa, they could not be distinguished anymore, indicating that the sample had undergone pressure amorphization. No evidence of further transformation was observed up to 8 GPa. Upon pressure release, the high-pressure amorphous phase was retained at ambient conditions. In principle, one could argue that the featureless spectrum in Fig. 1H could be the result of a large number of overlapped Bragg peaks from a low-symmetry structure, which were not resolved because of the intrinsically low resolution of the experimental technique. To clarify this point, we produced a greater amount of ZrW_2O_8 in the amorphous phase by compressing cubic ZrW_2O_8 at 7.5 GPa, using a toroidal high-pressure apparatus (*16*, *17*). For this compressed sample, a conventional angular-dispersive x-ray diffraction pattern could be obtained (Fig. 2) (*18*). The diffraction pattern (Fig. 2B) is typical for amorphous material and is in complete agreement with the energy-dispersive spectrum at 3.5 GPa (Fig. 1H), confirming that the latter indeed results from pressure-induced amorphization.

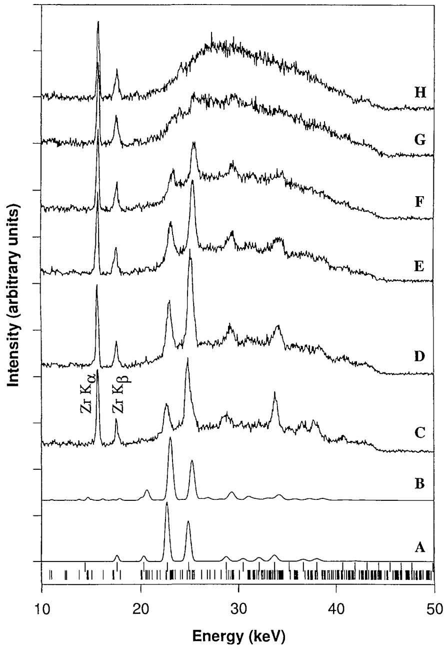

Fig. 1. EDXRD spectra of ZrW_2O_8 at increasing pressures in the DAC. Simulated spectra of (**A**) cubic and (**B**) orthorhombic phases of ZrW_2O_8 at ambient conditions. Spectra of ZrW_2O_8 at (**C**) 0, (**D**) 0.3, (**E**) 1.0, (**F**) 1.8, (**G**) 2.4, and (**H**) 3.5 GPa. All spectra were normalized to the Zr Kα fluorescence peak at 15.7 keV. Tick marks at the bottom of the figure indicate the expected positions of the Bragg peaks in both cubic and orthorhombic phases of ZrW_2O_8 at ambient pressure.

Raman spectroscopy was used to probe the structure of ZrW_2O_8 at a molecular length scale during the pressure-induced amorphization. Factor group analysis of cubic ZrW_2O_8 (space group $P2_13$) in the long wavelength limit provides a decomposition in irreducible representations according to $11A$ (R) + $11E$ (R) + $32T$ (R, IR), where A, E, and T represent nondegenerate, doubly degenerate, and triply degenerate optical modes, respectively. R and IR stand for Raman and infrared active modes, respectively. In the Raman spectra at ambient conditions of α-ZrW_2O_8 (cubic phase) and γ-ZrW_2O_8 (orthorhombic phase) (Fig. 3, A and B, respectively), a total of 13 and 22 Raman active modes, respectively, were identified above 200 cm^{-1} (Table 1). The values for the cubic phase are in excellent agreement with those previously reported by Evans *et al.* (*7*); we are not aware of previous publication of the Raman frequencies for γ-ZrW_2O_8.

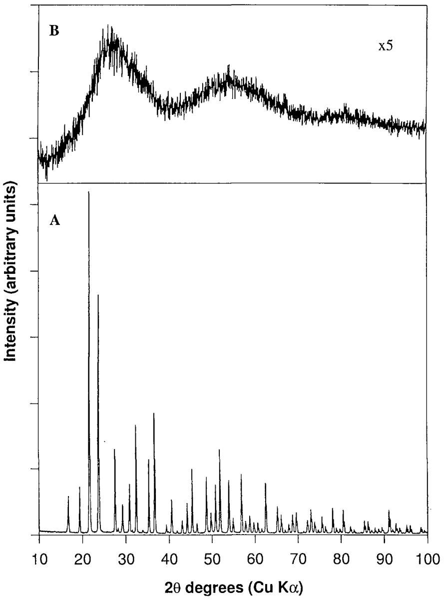

Fig. 2. X-ray diffraction pattern at ambient conditions of (**A**) α-ZrW_2O_8 as prepared and (**B**) amorphous ZrW_2O_8 recovered after compressing α-ZrW_2O_8 to 7.5 GPa in a toroidal chamber. The counts in (B) were multiplied by 5. For comparison, the first broad maximum in (B) corresponds to an energy range from 20 to 40 keV in Fig. 1H.

The Raman spectrum of zirconium tungstate shows some degree of local disordering even at pressures as low as 0.2 GPa. Above 0.2 GPa, the onset of the cubic-to-orthorhombic phase transition was revealed most notably by the splitting of the Raman peaks at 735 and 790 cm^{-1}, attributed to the lowering of tungsten site symmetry from C_3 in cubic $P2_13$ to C_1 in orthorhombic $P2_12_12_1$. At increasing pressures, the Raman spectrum of ZrW_2O_8 became increasingly diffuse, and above 3 GPa, the peaks from the orthorhombic phase collapsed into two very broad peaks at about 800 and 1000 cm^{-1} (Fig. 4), indicating pressure-induced amorphization. As in the case of the x-ray diffraction results, the Raman spectrum after pressure release shows that the high-pressure amorphous phase is retained at ambient conditions.

Amorphous ZrW_2O_8 was annealed at ambient pressure in air during periods of 1 hour at increasing temperatures. The sam-

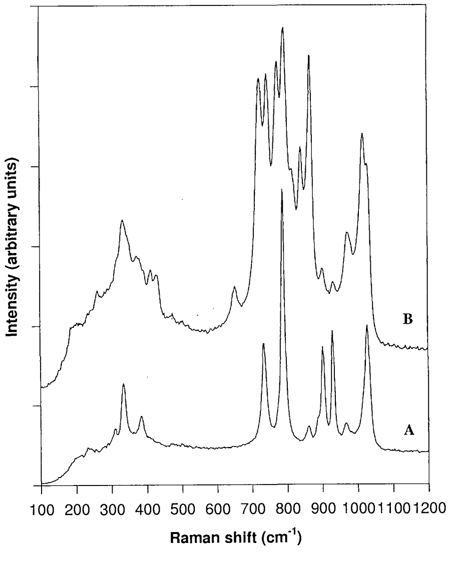

Fig. 3. Raman spectra at ambient conditions of (**A**) α-ZrW_2O_8 and (**B**) γ-ZrW_2O_8 quenched from 1.0 GPa. Note the splitting of the peaks around 750 cm^{-1} in going from the cubic to the orthorhombic phase.

ple remained in the amorphous state up to 873 K. A further increase in the annealing temperature to 923 K promoted the recrystallization of amorphous ZrW_2O_8 to its original cubic structure. This result indicates that the kinetic barrier of recrystallization is almost as high as that of decomposition of ZrW_2O_8 into ZrO_2 and WO_3. Indeed, by heating amorphous ZrW_2O_8 to 973 K, we observed not only recrystallization of the cubic phase but also decomposition, as revealed by the presence of tungsten trioxide peaks in the Raman spectrum.

Both Raman and x-ray diffraction data show that pressure amorphization of ZrW_2O_8 occurs progressively, starting at about 1.5 GPa and extending over a pressure range of more than 1.5 GPa. The amorphization of zirconium tungstate occurs at a pressure far below that of the great majority of the other compounds that also undergo pressure amorphization. We also observed that amorphization of ZrW_2O_8 can be induced by heavy grinding in an agate mortar.

Our results, the presence of QRUMs in ZrW_2O_8 (*9*), and the relatively small bulk modulus of cubic and orthorhombic phases (*8*) all suggest that the compression mechanism in ZrW_2O_8 up to 1.5 GPa should involve both polyhedral tilting and slight distortion of the polyhedral units, without bond breaking. This hypothesis is supported by the fact that neither x-ray diffraction nor Raman data below 1.5 GPa provide any evidence of a major change in the first coordination polyhedra. At this stage, some of the QRUMs eigenvectors could provide an energetically convenient route to reduce the framework volume. In these transversal modes, the polyhedral units periodically run across a transient point of minimal bent and greater volume. Consequently, the energy barrier for polyhedra crossing from one orientation to another will increase with pressure, leading eventually to a freezing of the polyhedra into particular orientations. Because of the natural flexibility of the ZrW_2O_8 framework, a great number of low-energy phonon states will be populated at ambient temperature, and the ZrO_6 and WO_4 units will be frozen into an orientationally disordered state at increasing pressure (*19*). Above 1.5 GPa, further volume reduction in zirconium tungstate will occur simultaneously with a greater deformation of the polyhedral units, leading ultimately to the collapse of the framework into an amorphous high-pressure phase, probably accompanied by changes in cation coordination, as suggested by the high kinetic barrier of recrystallization of the amorphous phase. In this scenario, negative thermal expansion and pressure-induced amorphization are both related to the intrinsic high flexibility of the ZrW_2O_8 framework.

The observed amorphization at relatively low pressures of zirconium tungstate, a mixed tetrahedral-octahedral network structure, extends previous model predictions restricted to tetravalent networks (*4*) and suggests a general trend between negative thermal expansion and pressure-induced amorphization in highly flexible framework structures.

Table 1. Raman frequencies of α-ZrW_2O_8 and γ-ZrW_2O_8 at ambient conditions. s, strong; m, medium; w, weak; v, very; br, broad.

Raman shift (cm^{-1})	
α-ZrW_2O_8	γ-ZrW_2O_8
236 vw	263 w
308 vw	318 w
334 m	334* m, br
384 m	376 w, br
	392 w
	413 w
	430 w
	653 w
735 m	722 m
	746 m
790 s	774 m
	795 m
	816 w
	841 m
860 w	867 m
887 w	
902 m	902* w
	919 vw
930 m	931* w
969 w	974 m
	982 w
1019 w	1018 m
1029 m	1033 m

*Probable contamination of cubic phase not transformed or reconverted by laser heating.

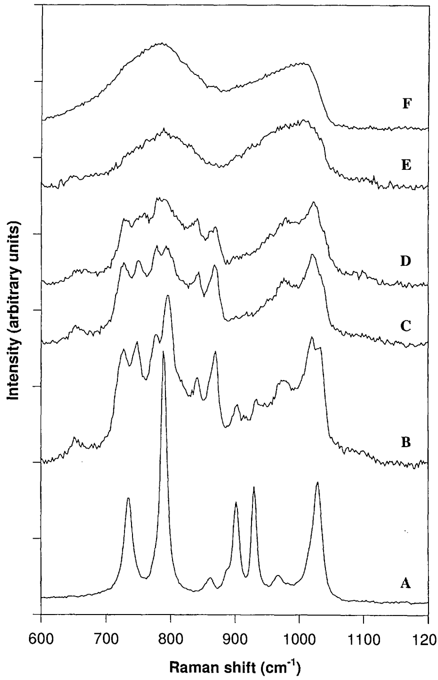

Fig. 4. Pressure dependence of the Raman spectra of ZrW_2O_8. (**A**) Sample at ambient conditions. Spectra taken in the DAC at (**B**) 0.22, (**C**) 0.75, (**D**) 1.6, and (**E**) 3.2 GPa. (**F**) Spectrum at zero pressure of the sample recovered after compressing.

REFERENCES AND NOTES

1. See, for example, J. S. Tse and D. D. Klug, *Phys. Rev. Lett.* **70**, 174 (1993); J. S. Tse, *J. Chem. Phys.* **96**, 5482 (1992); F. Sciortino *et al.*, *Phys. Rev. E* **52**, 6484 (1995); A. G. Lyapin and V. V. Brazhkin, *Phys. Rev. B* **54**, 12036 (1996).
2. See, for example, M. B. Kruger and R. Jeanloz, *Science* **249**, 647 (1990); J. S. Tse, D. D. Klug, J. A. Ripmeester, S. Desgreniers, K. Lagarec, *Nature* **369**, 724 (1994); O. Mishima, *ibid.* **384**, 546 (1996); C. Meade, R. J. Hemley, H. K. Mao, *Phys. Rev. Lett.* **69**, 1387 (1992); G. C. Serghiou, R. R. Winters, W. S. Hammack, *ibid.* **68**, 3311 (1992); J. H. Nguyen, M. B. Kruger, R. Jeanloz, *ibid.* **78**, 1936 (1997); P. Gillet, J. Badro, B. Varrel, P. F. McMillan, *Phys. Rev. B* **51**, 11262 (1995).
3. Y. G. Gogotsi, A. Kailer, K. G. Nickel, *Mater. Res. Innovat.* **1**, 3 (1997).
4. R. J. Speedy, *J. Phys. Condens. Matter* **8**, 10907 (1996).
5. C. Martinek and F. A. Hummel, *J. Am. Ceram. Soc.* **51**, 227 (1968).
6. T. A. Mary, J. S. O. Evans, T. Vogt, A. W. Sleight, *Science* **272**, 90 (1996).
7. J. S. O. Evans, T. A. Mary, T. Vogt, M. A. Subramanian, A. W. Sleight, *Chem. Mater.* **8**, 2809 (1996).
8. J. S. O. Evans *et al.*, *Science* **275**, 61 (1997).
9. A. K. A. Pryde *et al.*, *J. Phys. Condens. Matter* **8**, 10973 (1996).
10. For reviews on RUMs, see M. T. Dove, *Am. Mineral.* **82**, 213 (1997); K. D. Hammonds, M. T. Dove, A. P. Giddy, V. Heine, B. Winkler, *ibid.* **81**, 1057 (1996); M. T. Dove, V. Heine, K. D. Hammonds, *Mineral. Mag.* **59**, 629 (1995).
11. J. Graham, A. D. Wadsley, J. H. Weymouth, L. S. Williams, *J. Am. Ceram. Soc.* **42**, 570 (1959); L. L. Y. Chang, M. G. Scroger, B. Phillips, *ibid.* **50**, 211 (1967). ZrW_2O_8 was prepared by heating a mixture of ZrO_2 and WO_3 in the correct stoichiometric proportion in a sealed platinum tube at 1473 K for 48 hours. Cubic ZrW_2O_8 was retained metastably at ambient conditions by quenching the sample in water. Rietveld analysis of the x-ray diffraction pattern of the product revealed essentially pure cubic ZrW_2O_8, with a residual amount of less than 1.7% of ZrO_2.
12. EDXRD experiments were done with a liquid nitrogen-cooled, intrinsic germanium detector from Princeton Gamma Tech, with measured resolution of 163 eV at 5.894 keV. Radiation from a conventional tungsten x-ray tube, operating at 45 kV and 20 mA, was collimated to a beam of 160-μm diameter before reaching the sample in the DAC. The diffraction angle was kept fixed at 7.62°, and acquisition time was typically 24 hours for each spectrum. After each spectrum acquisition, the energy scale was calibrated against an ^{241}Am radioactive source to compensate for any drift of the amplifier electronics. Peak positions in the EDXRD spectra were determined by fitting the peaks to Gaussian profiles, with the program XRDA [S. Desgreniers and K. Lagarec, *J. Appl. Crystallogr.* **27**, 432 (1994)].
13. Raman spectra were obtained with a Raman microprobe consisting of an Olympus BH-2 microscope equipped with a holographic beam splitter and a super notch filter, a Jobin-Yvon HR320 monochromator, and a EG&G Princeton Applied Research charge-coupled device detector cooled with liquid nitrogen. A nominal 10-mW HeNe laser (632.8 nm) was used as the excitation source.
14. A Piermarini-Block DAC was used to generate high pressures [G. J. Piermarini and S. Block, *Rev. Sci. Instrum.* **46**, 973 (1975)]. The powder sample, together with a small ruby chip as a pressure gauge, was conditioned inside a hole of 250-μm diameter drilled in a

Waspaloy gasket preindented to 80 μm. No pressure medium was used. The low deviatoric stress condition inside the gasket hole was monitored by observing the broadening of the ruby peaks as pressure increased. Experiments performed with either methanol-ethanol-water (16:3:1) or silicon oil as the pressure medium yielded essentially the same results.
15. G. J. Piermarini, S. Block, J. D. Barnett, R. A. Forman, *J. Appl. Phys.* **46**, 2774 (1975).
16. A sample of ZrW_2O_8 of about 12 mm^3 was encapsulated into hexagonal boron nitride and put inside a gasket to guarantee quasi-hydrostatic conditions during the experiment. Pressure was calibrated with the fixed points of bismuth [W. F. Sherman and A. A. Stadtmüller, *Experimental Techniques in High Pressure Research* (Wiley, New York, 1987), chap. 6]. After compression, the pellet of ZrW_2O_8 was carefully ground in an agate mortar to provide a powder sample suitable for x-ray diffractometry.
17. L. G. Khvostantsev, *High Temp. High Pressures* **16**, 165 (1984).
18. X-ray powder diffraction data for the cubic and amorphous samples of ZrW_2O_8 at ambient conditions were obtained with a Siemens D500 diffractometer equipped with Soller slits in the incident beam, a 1° divergence slit, a 0.15-mm receiving slit, and a graphite monochromator in the secondary beam. Data were collected with Cu Kα radiation, in the angular range from 10° to 100° (2θ°), with a step scan of 0.05° and an acquisition time of 2 s by step (1 s for the cubic zirconium tungstate sample).
19. A similar mechanism of pressure-induced amorphization can be found in the review by S. M. Sharma and S. K. Sikka [*Prog. Mater. Sci.* **40**, 1 (1996)].

20. We thank J. Haines from the Laboratoire de Physico-Chimie des Matériaux–CNRS, Meudon (France) for a critical review of the paper and M. Sasso for help with the toroidal chamber. This work was supported by Conselho Nacional de Desenvolvimento Científico e Tecnológico (CNPq), Financiadora de Estudos e Projetos (FINEP), Fundação de Amparo à Pesquisa do Estado do Rio Grande do Sul (FAPERGS), and Perto S.A. (Brazil).

11 December 1997; accepted 17 March 1998

Self-Trapping of Dark Incoherent Light Beams

Zhigang Chen, Matthew Mitchell, Mordechai Segev,
Tamer H. Coskun, Demetrios N. Christodoulides

"Dark beams" are nonuniform optical beams that contain either a one-dimensional (1D) dark stripe or a two-dimensional (2D) dark hole resulting from a phase singularity or an amplitude depression in their optical field. Thus far, self-trapped dark beams (dark solitons) have been observed using coherent light only. Here, self-trapped dark incoherent light beams (self-trapped dark incoherent wavepackets) were observed. Both dark stripes and dark holes nested in a broad partially spatially incoherent wavefront were self-trapped to form dark solitons in a host photorefractive medium. These self-trapped 1D and 2D dark beams induced refractive-index changes akin to planar and circular dielectric waveguides. The experiments introduce the possibility of controlling high-power coherent laser beams with low-power incoherent light sources such as light emitting diodes.

Solitons have been intensively explored in many areas of physics. In optics, a soliton forms when an optical wavepacket (a pulse or a beam) propagates in a nonlinear medium while maintaining a constant shape without broadening. This is due to a balance between dispersion (in time) or diffraction (in space) and nonlinear "lensing" effects. In the spatial domain, self-trapping of a bright (or dark) optical beam can lead to a spatial soliton when the beam diffraction is counteracted by light-induced self-focusing (or self-defocusing). Thus far, self-trapping of dark beams (*1*), in the form of 1D dark stripes (*2–6*) or 2D "holes" (*7–11*), has been observed using spatially coherent light only. Nature, however, is full of incoherent light sources. In fact, most natural sources of electromagnetic radiation emit light that is incoherent either spatially or temporally, or both. Until recently, the commonly held impression was that solitons are exclusively coherent entities. Our group, however, has experimentally demonstrated that an incoherent light source can excite incoherent bright solitons in a nonlinear photorefractive medium (*12, 13*). These were the first observations of self-trapped incoherent wavepackets in nature. Incoherent solitons are altogether new entities, because their phase distribution is random. Following the observations of bright incoherent solitons, a natural question arises: Can such incoherent beams also support dark solitons?

On the basis of knowledge of coherent dark solitons (*1*), one may speculate that the transverse phase also plays a crucial role for incoherent solitons. Fundamental 1D coherent dark solitons require a transverse π phase shift at the center of the dark stripe, whereas an initially uniform transverse phase leads to a Y-junction soliton. Furthermore, 2D coherent dark solitons (vortex solitons) require a helical $2m\pi$ transverse phase structure (m = integer). Extending the idea of dark coherent solitons to dark incoherent solitons raises several questions. If dark incoherent solitons were to exist, is their phase structure important (as for coherent dark solitons) or irrelevant (as for bright incoherent solitons, upon which the phase is fully random)? And, if the phase does play a role, how can it be "remembered" by these incoherent entities throughout propagation? Altogether, even though it has been shown both experimentally (*12, 13*) and theoretically (*14–18*) that bright incoherent solitons exist, the existence of dark incoherent solitons is not at all clear. However, we found numerically (*19*) that when a dark stripe-bearing incoherent beam is launched into a noninstantaneous nonlinear medium (a biased photorefractive crystal), the beam undergoes considerable evolution but eventually stabilizes, with some small oscillatory "breathing," around a self-trapped solution. Surprisingly, we found that a single dark incoherent soliton requires an initial transverse π phase jump and that the dark incoherent soliton is always gray. In addition, in the extreme case of a very broad dark beam, Hasegawa found a closed-form solution for dark incoherent solitons in plasmas (*14*). These theoretical results, although not providing answers to the questions raised above, do suggest that dark incoherent solitons should exist.

Here, we report the experimental observation of self-trapping of dark partially spatially-incoherent light beams in the form of 1D dark soliton stripes and 2D soliton holes. To our knowledge, this is the first observation of self-trapping of dark incoherent wavepackets in nature.

A spatially incoherent beam is a "speckled" multimode beam of which the instantaneous intensity pattern consists of many speckles that vary randomly in time. Such an incoherent beam cannot self-trap in an instantaneous nonlinearity. If an incoherent beam is launched into an instantaneous nonlinear medium (for example, optical Kerr medium), each speckle forms a small lens and captures a small fraction of the beam, thus completely fragmenting the beam's envelope. On the other hand, if the nonlinearity is noninstantaneous with a response time that is much longer than the phase fluctuation time across the beam, then the medium responds to the time-averaged envelope and not to the instantaneous "speckles." Therefore, for an incoherent soliton, a noninstantaneous nonlinearity is required (*16*). A convenient choice for producing this state is photorefractive materials for which the optical illumination controls the response time of

---

Z. Chen, M. Mitchell, M. Segev, Electrical Engineering Department and Center for Photonics and Optoelectronic Materials (POEM), Princeton University, Princeton, NJ 08544, USA.
T. H. Coskun and D. N. Christodoulides, Department of Electrical Engineering and Computer Science, Lehigh University, Bethlehem, PA 18015, USA.